ELSEVIER

Journal of Power Sources 94 (2001) 212–218

JOURNAL OF POWER SOURCES

www.elsevier.com/locate/jpowsour

Concentration measurements in lithium/polymer–electrolyte/lithium cells during cycling

C. Brissot[a], M. Rosso[a,*], J.-N. Chazalviel[a], S. Lascaud[b]

[a]*Laboratoire de Physique de la Matière Condensée, Ecole Polytechnique-CNRS, 91128 Palaiseau, France*
[b]*EDF/DER, BP No. 1, 77250 Moret sur Loing, France*

Received 19 June 2000; accepted 24 July 2000

Abstract

We report on in situ and ex situ concentration measurements in lithium/polymer–electrolyte/lithium cells during cycling. We have used three different methods which give complementary results, in good agreement with theoretical predictions and previous concentration measurements by Raman confocal microspectroscopy. Our methods allow to obtain concentration maps in the electrolyte, in particular, when dendrites are observed: from these measurements, we can correlate the onset of dendritic growth with local concentration gradients.

Keywords: Lithium/polymer–electrolyte/lithium cells; Concentration measurement; Cycling

1. Introduction

The all-solid-state lithium battery is considered as one of the promising technologies to meet the requirements of upcoming applications of electric power sources (such as portable electronic devices or electrical vehicles). In this framework, a large interest has been devoted to lithium metal/polymer batteries [1,2]. In principle, metallic lithium is a good candidate for the anode, since it has a very high theoretical specific capacity: however, the formation of dendrites affects the cyclability of this type of electrode. Hence, a complete understanding of this effect is crucial for optimizing the operation of all-solid-state lithium batteries.

It has been predicted theoretically [3], and several authors have reported that, when depositing a metal from a binary electrolyte, dendritic growth starts when the concentration of metal ions approaches 0 at the negative electrode [4–7]. Also, inhomogeneities in salt concentration are expected to enhance or accelerate dendritic growth in these systems, because these inhomogeneities may induce large fluctuations in the current density. Hence, in situ concentration measurements should provide very useful informations on dendritic growth mechanisms. Such measurements have been made by several authors for different systems, but there are few experimental results in lithium/polymer batteries. Recently, Rey et al. have measured concentration profiles in a poly(ethylene oxide) (PEO) electrolyte by in situ Raman confocal microspectroscopy, in symmetric lithium/polymer–electrolyte/lithium cells [8,9]: the profiles were in good agreement with theoretical predictions of Brissot et al. [10], and allowed to make a precise determination of physical parameters of the electrolyte, such as the diffusion constants or the ionic transport numbers. Preliminary results were also obtained in lithium/polymer–electrolyte/insertion cathode cells [9]. Technical limitations did not permit as precise measurements as in symmetric cells: however, the obtained concentration profiles were in qualitative agreement with concentration profiles calculated by Doyle et al. [11].

In a recent paper [12], we have reported on optical concentration measurements in symmetric lithium/$(PEO)_{20}$–LiTFSI/lithium cells. Three different methods were used. Two of these methods were in situ methods, measuring either optical absorption of the electrolyte, or optical index gradients. The last method was based on the variation of a phase-transition temperature with salt concentration [13–15]. All of these methods allowed to obtain concentration maps in the cells, hence, were able to detect and follow concentration inhomogeneities within the electrolyte.

Here, we will present a summary of our experimental techniques and our main results (Section 3). These will be

* Corresponding author. Tel.: +33-1-69-33-4667; fax: +33-1-69-33-3004.
E-mail address: michel.rosso@polytechnique.fr (M. Rosso).

0378-7753/01/$ – see front matter
PII: S0378-7753(00)00589-9

compared to the results of a simple one-dimensional model (Section 2).

2. Model

Let us consider the evolution of the anionic and cationic concentrations C_a and C_c in a binary electrolyte submitted to a constant current density J, in a parallepipedic cell. We may assume that our system is described by the following set of equations [10,12]

$$\frac{\partial C_c}{\partial t} = -\text{div}\, W_c \tag{1}$$

$$\frac{\partial C_a}{\partial t} = -\text{div}\, W_a \tag{2}$$

$$W_c = -D_c \,\text{grad}\, C_c + \mu_c C_c E \tag{3}$$

$$W_a = -D_a \,\text{grad}\, C_a - \mu_a C_a E \tag{4}$$

here subscripts c and a refer to cations and anions, respectively, W is the ionic fluxes, D the diffusion constants, μ the mobilities and E the electric field. In the following, we assume that the electrolyte remains neutral, i.e. $z_a C_a \approx z_c C_a \approx C$, where z_a and z_c are the anionic and cationic charge numbers, respectively. We also consider the simple case where the cell is uniform in both directions parallel to the electrodes. Then the set of Eqs. (1)–(4) may be written as a function of a single space coordinate x, in the direction perpendicular to the electrodes.

If we now suppose that the diffusion constants and mobilities are independent of concentration, Eqs. (1)–(4) can be simply combined as follows.

$$\frac{\partial C}{\partial t} = D_c \frac{\partial^2 C}{\partial x^2} + \mu_c \frac{\partial}{\partial x}\left(C \frac{\partial V}{\partial x}\right) \tag{5}$$

$$\frac{\partial C}{\partial t} = D_a \frac{\partial^2 C}{\partial x^2} - \mu_a \frac{\partial}{\partial x}\left(C \frac{\partial V}{\partial x}\right) \tag{6}$$

where V is the electrostatic potential. Elimination of the potential-dependent term leads to a simple ambipolar diffusion equation

$$\frac{\partial C}{\partial t} = D \frac{\partial^2 C}{\partial x^2} \quad \text{with} \quad D = \frac{D_a \mu_c + D_c \mu_a}{\mu_c + \mu_a} \tag{7}$$

Considering that, at the negative electrode ($x = 0$) and at the positive electrode ($x = L$), the current density is only due to cations ($W_c(0) = W_c(L) = J/e$ and $W_a(0) = W_a(L) = 0$, with $J < 0$), we obtain for the boundary conditions

$$\frac{\partial C}{\partial x}(x = 0) = \frac{\partial C}{\partial x}(x = L) = \frac{-J}{eD(1 + \mu_c/\mu_a)} \tag{8}$$

where e is the elementary charge.

As discussed in [12,16], the assumption that the diffusion constants and mobilities are independent of concentration is quite unrealistic. In fact, in (PEO)–LiTFSI, the diffusion constants and mobilities strongly depend on the ionic concentration [10,13,14]. Now, at high current density, the ionic concentration at the negative electrode eventually decreases to a value close to 0: then, the diffusion constant in this region is very different from the initial diffusion constant. In order to give a better description of our system, we have taken into account the variations of the diffusion constant with concentration in Eqs. (1)–(4), deduced from the conductivity measurements reported by Lascaud et al. [13]. From Eqs. (1)–(4), taking $J = z_c e W_c - z_a e W_a$, and assuming Einstein's relation to hold, we, then, obtained the following set of equations, that we could solve numerically

$$\frac{\partial C}{\partial t} = -\text{div}\, W_a = -\text{div}\, W_c \tag{9}$$

$$W_a = -D(x) \,\text{grad}\, C - \frac{\mu_a(x)}{\mu_a(x) + \mu_c(x)} \frac{J}{z_a e} \tag{10}$$

where the diffusion constant D and mobilities μ_a and μ_c now depend on C, and therefore, are functions of x.

Moreover, as previously shown in [10,16], variations of the ionic concentration in the vicinity of the electrodes induce a global motion of the electrolyte toward the negative electrode. This motion is related to the change of the polymer density. It contributes to the displacement of the ions and has to be taken into account. We have also included this effect in our calculation, using the method explained in [10].

In the next section, we will compare the results of this calculation to our experimental measurements.

3. Experiments

Our concentration measurement experiments have been reported in detail in [12]. We will briefly present here our experimental techniques and discuss our main results.

3.1. Experimental conditions

The polymer electrolyte consists of poly(ethylene oxide) ($MW = 3 \times 10^5$). In most experiments the lithium salt is $LiN(CF_3SO_2)_2$ (abbreviated in LiTFSI), discovered by Armand et al. [17]. In one series of experiments (see below), LiNPSI [$LiN(p\text{-}NO_2C_6H_4SO_2)_2$] [18,19] is added to this electrolyte, to form a 50 mole% LiNPSI–50 mole% LiTFSI mixture. In all cases, the salt concentration in terms of O/Li ratio is about 20. Preparation details have been given elsewhere [12].

The experimental cell is schematically shown in Fig. 1. The cell is made of two glass plates: the lower plate has a 1 cm width and a 0.07 cm depth channel in which the two lithium foils are pushed against the electrolyte. The upper plate has a T-shape that fits in the channel of the lower plate. The distance between the two electrodes is about 1 mm. The whole lithium/polymer–electrolyte/lithium assembly and nickel collectors are maintained by the upper plate of the

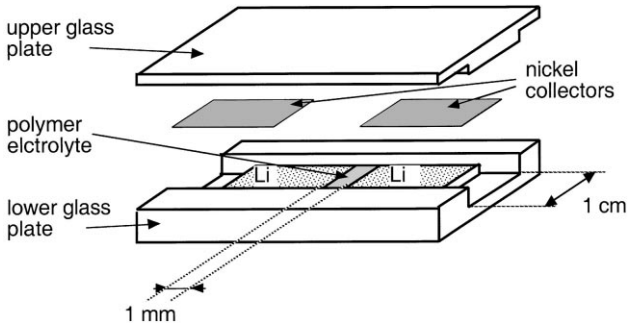

Fig. 1. A schematic view of the electrochemical cell.

cell. The two plates are sealed together with a resin in order to avoid contamination of lithium by ambient air. The cell is assembled in an argon-filled dry box. The nickel collectors are connected to a standard electrochemical set-up (Schlumberger's 1286 electrochemical interface and 1250 frequency response analyzer).

The cell is put in a furnace and heated at 80°C. At this temperature, we measure a conductivity of 9.1×10^{-4} S cm^{-1}. The cells are polarized under galvanostatic conditions, with current densities in the range 0.1–2 mA cm^2. Our furnace has windows allowing observation of the inter-electrode space.

The evolution of the dendrites is monitored by a black and white charge coupled device (CCD) camera fitted on a microscope. Pictures are digitized with a Perceptics Pixelpipe framegrabber, and recorded on a Macintosh microcomputer. They are subjected to standard image analysis using National Institute of Health (NIH) Image software. In particular, it is possible to correct non uniformities of our optical set-up by comparing the images of interest to a reference image (usually the image before applying the polarization).

Usually, when a cell is polarized for the first time at a high current density (typically $J > 0.3$ mA cm^{-2}), no dendrites are observed [10]: the ionic concentration in the vicinity of the negative electrode decreases [20,21], cations are plated, forming a compact metallic layer on the electrode, whereas anions drift toward the positive electrode. This results in concentration gradients in the neighborhood of both electrodes. Then, during subsequent polarizations of the cell, dendrites may start growing. We will examine separately in the following: (i) the simpler situation before any dendrite has appeared; (ii) the evolution of the concentration map at and after the onset of dendritic growth.

3.2. Concentration profiles in the absence of dendrites

3.2.1. In situ optical absorption

Optical absorption is a very simple and direct method for measuring the concentration in a material. For example, in situ measurements of the optical absorption due to Cu^{2+} ions have already been reported in $Cu/CuSO_4/Cu$ cells [5,22]: this method has allowed to measure very precisely the concentration maps in the electrolyte during the polarization of these cells. However, TFSI has no absorption in the spectral region that is available for our optical set-up. On the other hand, we have found that the $NPSI^-$ anion discovered by Reibel et al. [18,19] has an absorption band in the region around 400 nm [12]. Because, $(PEO)_n$–LiNPSI does not adhere well on the electrodes, we have used a 50 mole% LiNPSI–50 mole% LiTFSI mixture. A cell filled with this compound was illuminated with a blue mercury-vapor lamp emitting in the 400 nm range. Then, during the polarization, changes in the $NPSI^-$ concentration within the electrolyte resulted in changes of its optical absorption. These changes were simply measured using our CCD camera. We assumed a linear relationship between the absorption and the ionic concentration. Although no specific experiment was performed to check this particular point, all our results were compatible with this assumption [12].

Fig. 2(a) shows a picture taken during a polarization at a current density $J = 0.95$ mA cm^{-2}. Soon after the onset of the polarization, one clearly sees a lighter region in the vicinity of the negative electrode due to the low concentration of $NPSI^-$ in this region. Similarly, one can see a darker region in the vicinity of the positive electrode, corresponding to an increase of the $NPSI^-$ concentration.

From Fig. 2(a), one can measure an optical density profile, which is very similar to the calculated concentration profile (Fig. 2b), obtained for the following set of parameters: $O/Li = 20$, $J = 0.95$ mA cm^{-2}, inter-electrode distance $L = 1.32$ mm, electrolyte conductivity $\sigma = 3.1\times 10^{-4}$ S cm^{-1}. In particular, the experimental and calculated widths of the diffusion regions are very similar. This result shows that the optical absorption technique may provide a very simple and direct method for measuring concentration changes in the electrolyte.

However, we have encountered two difficulties. The first difficulty is related to the fact that we have to deal with a rather complex electrolyte, with three different types of ions. In particular, we do not know the transport numbers of these three ions. As a consequence, the model presented in Section 2 does not apply to our electrolyte. As explained in [12], we had to use a very crude approximation, replacing the ($TFSI^-$, $NPSI^-$) pair by an ''effective anion'', whose properties were determined from the electrical conductivity and Sand's behavior [23] of our system. The curve shown in Fig. 2b has been calculated for this effective anion.

The second difficulty comes from the occurrence of irreversible changes that we observed in the electrolyte in the vicinity of the negative electrode: we have attributed this behavior to a change in the structure of the electrolyte, occurring at low concentration. At the temperature of our experiments (80°C), we have calculated that this change occurred when the concentration was in the range $20 \leq O/Li \leq 30$. This of course limits the application of the optical absorption method to a restricted range of experimental conditions.

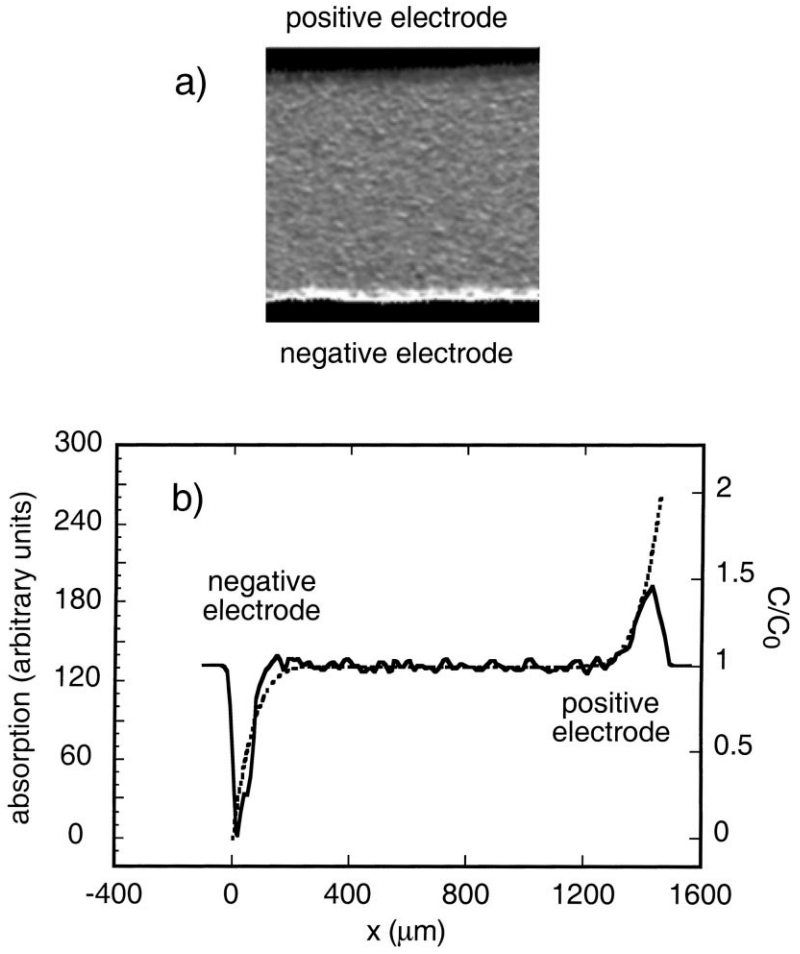

Fig. 2. (a) Optical absorption in a PEO–LiNPSI/LiTFSI electrolyte. The cell has been polarized for 820 s, at a current density $J = 0.95$ mA cm^{-2}. The light region corresponds to the low NPSI$^-$ concentration region, while the dark region corresponds to the high NPSI$^-$ concentration region. (b) Absorption profile in the electrolyte, measured from the picture shown in (Fig. 2a) (solid line). The dashed line shows the profile calculated using the model described in Section 2.

We have then investigated two other methods to determine concentration maps, which both may be applied to the more conventional PEO–LiTFSI electrolyte.

3.2.2. *In situ gradient-sensitive optical detection*

Illumination of a cell with a monochromatic, parallel light, at a small angle θ_i with the direction perpendicular to the cell, permits to measure changes of the optical index related to concentration gradients [12]: such an effect has already been reported in the literature for a different system [24]. In our experiment, the angle θ_i was 5°.

The ionic concentration increases (decreases) in the vicinity of the positive (negative) electrode: hence, the concentration gradient has the same sign at both electrodes. As a consequence, if the optical index is a monotonous function of concentration, we expect that the gradient-sensitive optical detection technique will essentially evidence two darker or lighter regions close to the electrodes, depending on the angle θ_i between the incident light beam and the direction perpendicular to the electrodes. This is confirmed in our experiments (Fig. 3).

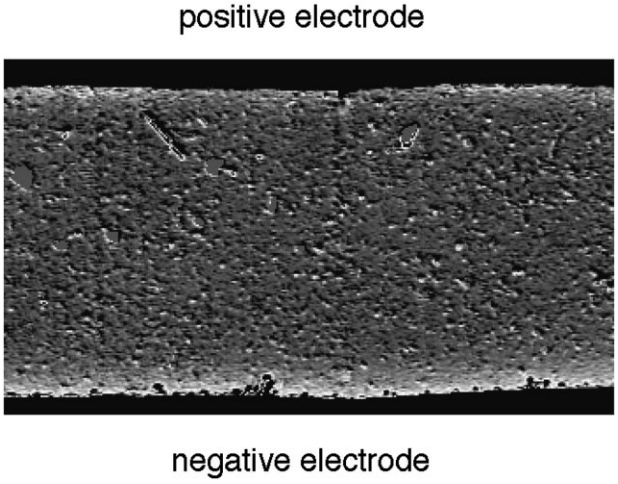

Fig. 3. Light intensity transmitted by the polymer electrolyte illuminated with a monochromatic, parallel light, at a small angle with the direction perpendicular to the cell (here the cell has been polarized for 2350 s at $J = 0.66$ mA cm^{-2}). In the vicinity of both electrodes, one observes two lighter regions, due to concentration changes inducing a variation of the optical index. The width of these lighter zones (∼120 μm) is almost equal to the diffusion length $\sqrt{(Dt)} \sim 140$ μm [32].

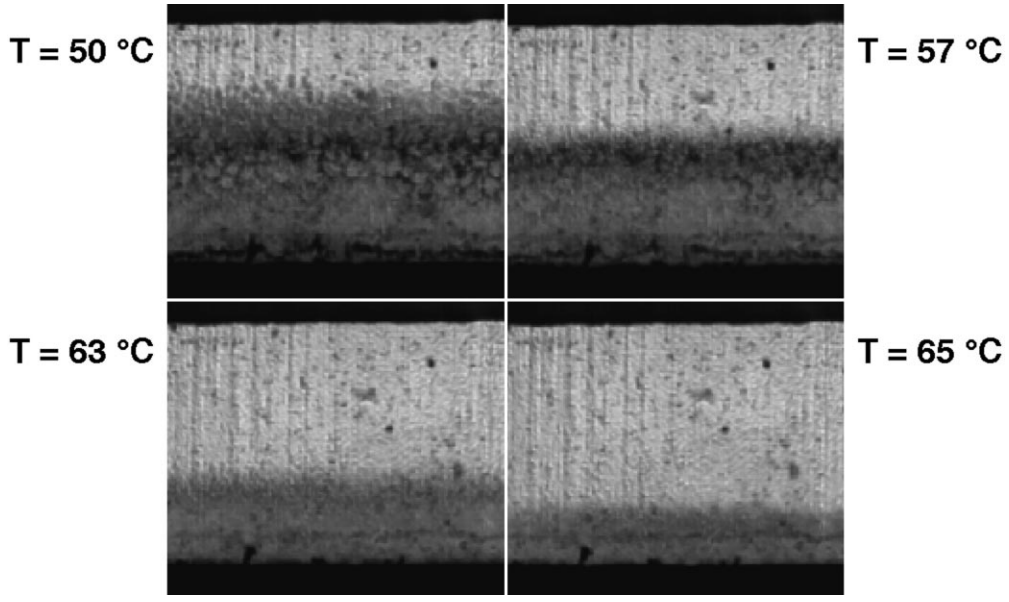

Fig. 4. At a given temperature the, boundary between the crystalline and the molten regions in the electrolyte corresponds to an isoconcentration line. This boundary can easily be observed as it corresponds to the frontier between the opaque and the transparent regions in the electrolyte. Here, we follow the evolution of the frontier between the transparent and opaque regions, at four successive temperature steps 50, 57, 63 and 66°C.

In fact, this method only gives qualitative information on concentration changes in the cell. First, one can easily show that this technique is also sensitive to higher order terms of the optical index gradients: $(dn/dx)^2$, d^2n/dx^2. Also, our system is not exactly two dimensional: the cell thickness is approximately 0.2 mm, whereas the distance between the electrodes is close to 1 mm. Hence, the ratio between the horizontal and vertical sizes is not very large. Moreover, we have observed that, very often, our systems are far from being uniform: indeed, local inhomogeneities at the surface of the electrodes [25,26] or in the electrolyte are expected to induce local variations of the current density, hence of the concentration gradients. Finally, it is important to stress that the gradient-sensitive optical detection method is more suitable for systems, where optical index gradients are large, hence, where concentration gradients are large: in our systems this is obtained for high current densities (in the mA cm^{-2} range or above).

However, the width of the perturbed region gives a good approximation for the diffusion length (Fig. 3). Also, we can deduce from our experiments the regions where the electrodes are the most active (see below).

3.2.3. Thermal method

Labrèche et al. [15] have studied the phase diagram of $(PEO)_n$–LiTFSI: for PEO with a high molecular weight

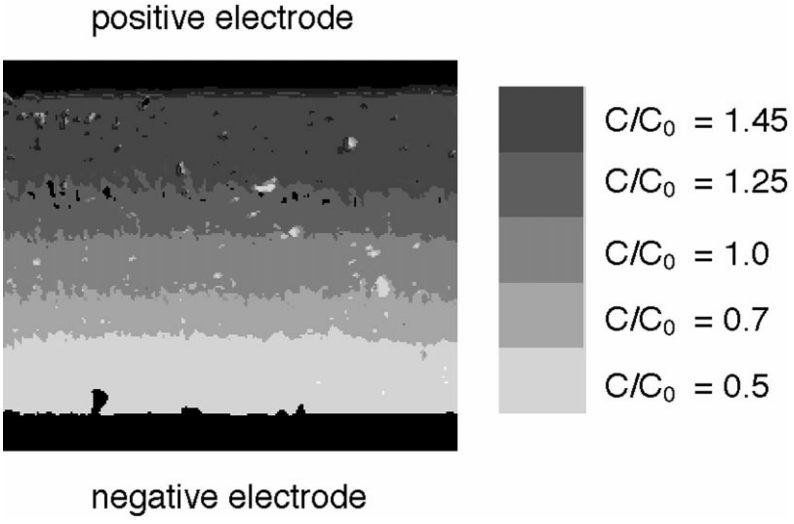

Fig. 5. From pictures taken at different temperatures, we can reconstruct the concentration map in the electrolyte. In this figure, only a limited number of grey levels are shown, evidencing isoconcentration lines.

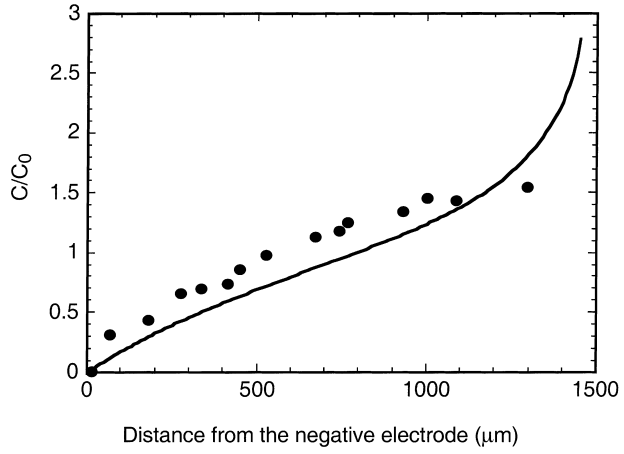

Fig. 6. The concentration profile deduced from pictures obtained at 15 different temperatures (closed circles) is in good agreement with the calculated profile (solid line).

(MW $= 4 \times 10^6$), at concentrations lower than the concentration corresponding to O/Li $= 6$, they observed a transition between a crystalline phase at low temperature ($T < T_m$) and a molten phase at high temperature. The temperature T_m was shown to decrease with increasing concentration [15].

We have used this variation to measure concentration changes in the electrolyte. The method consists essentially in detecting the position of the interface between the molten and the crystalline regions at different temperatures [12]. This detection is made easy because of the difference in optical transparency between the two phases.

We recall here the principle of the experiment. We first polarize a cell at 80°C. Then, we cool the cell very quickly, in order to quench the concentration distribution. Most of the electrolyte returns to its crystalline state. Then, we heat the cell with increasing temperature steps, and take pictures at these different temperatures: each of these pictures permits to determine an isoconcentration contour, corresponding to the line separating the transparent and the opaque regions.

For example, Fig. 4 shows a series of pictures of the inter-electrode space taken at four different temperatures: the cell shown in these pictures had been polarized at $J = 0.2$ mA cm^{-2}. For each picture, we observe two regions: a lighter one close to the positive electrode at the top and a darker one close to the negative electrode at the bottom. According to the phase diagram mentioned above, the transparent region corresponds to the higher concentration region. The line separating the lighter and the darker regions may be associated with a concentration C, which is determined from the temperature T. From such pictures, we can reconstruct the concentration map shown in Fig. 5. More precisely, we can determine the concentration profile in the inter-electrode space, and compare it with the results of our calculation (Fig. 6). We find a reasonable agreement between experimental and calculated data.

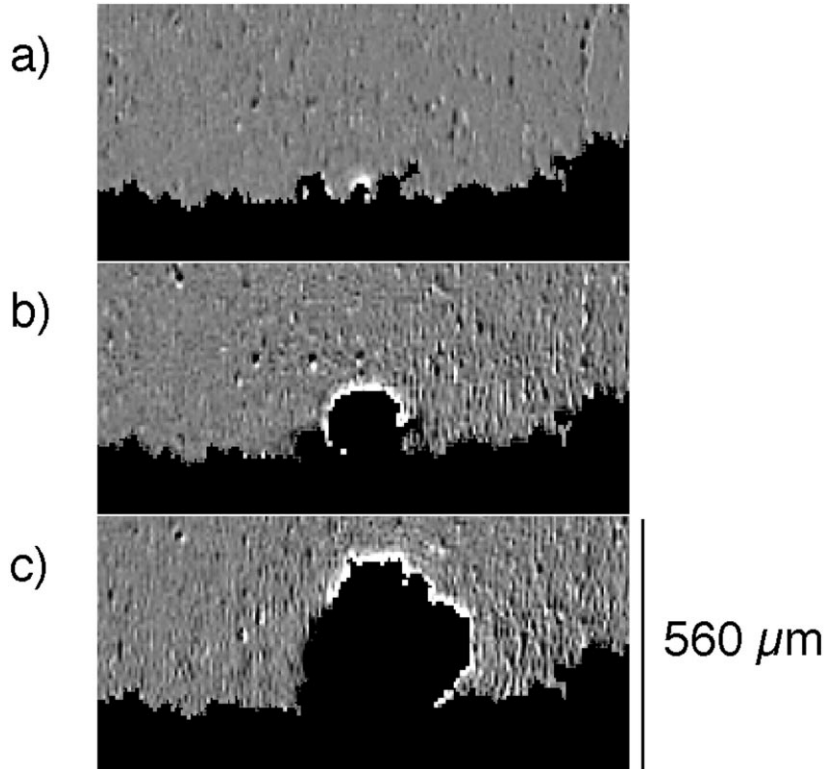

Fig. 7. Concentration gradient observed by the gradient-sensitive optical method, at $J = 0.7$ mA cm^{-2}, at successive time steps after the onset of polarization (a: 1800 s; b: 1920 s; c: 2280 s). These pictures evidence the existence of large concentration gradients in the vicinity of the growing dendrite.

Now, we must remember that, during the heating of the cell, diffusion will tend to smooth the concentration profiles. Then, we cannot observe the exact concentration map that was quenched at the end of a polarization. This is an intrinsic difficulty which limits the application of this method to experiments with relatively low concentration gradients [12].

3.3. Concentration maps around the dendrites

3.3.1. Before the onset of growth

Our concentration measurement methods allow to visualize concentration inhomogeneities in the electrolyte. For example, Fig. 7a–c were obtained with the gradient-sensitive method: they clearly show that the only dendrite that we observe in this series of pictures grows in the region where the concentration gradient is the highest (white color), hence, in the region where the concentration is lower. This also corresponds to the most active part of the electrode (J maximum). The optical absorption method permits similar observations.

3.3.2. During the growth

The three methods show similar concentration maps around the growing dendrites: for example, in Fig. 7, one observes large concentration gradients, hence, a depleted region around the dendrites. This is quite comparable to what has been observed in liquid binary electrolytes [4–6,23,27–31].

4. Conclusions

In this paper, we have presented three different techniques to measure concentration maps in lithium/polymer cells, which were shown to provide valuable information on these systems. In particular, we have demonstrated the correlation between dendritic growth and the existence of concentration gradients.

For different reasons, these three methods have intrinsic limitations: nevertheless, they give complementary results, which are in good agreement with theoretical predictions and previous concentration measurements by Raman confocal microspectroscopy. We are currently working on technical improvements of these methods.

The measurements described in this paper have been performed in symmetric lithium/polymer–electrolyte/lithium cells. They will be explored in other systems, in particular in lithium/polymer–electrolyte/insertion cathode cells, which are more similar to actual batteries.

References

[1] M. Gauthier, A. Bélanger, B. Kapfer, G. Vassort, in: J.R. Mac Callum, C.A. Vincent (Eds.), Polymer Electrolyte Reviews-2, Elsevier, London, 1989, p. 285.
[2] M.B. Armand, J.-Y. Sanchez, M. Gauthier, Y. Choquette, in: J. Lipkowski, P.N. Ross, (Eds.), Electrochemistry of Novel Materials, Frontiers of Electrochemistry, VCH, New York, 1994.
[3] J.-N. Chazalviel, Phys. Rev. A 42 (1990) 7355.
[4] R.H. Cork, D.C. Pritchard, W.Y. Tam, Phys. Rev. A 44 (1991) 6940.
[5] J.-N. Chazalviel, V. Fleury, M. Rosso, in: Trends in Electrochemistry, Council of Scientific Research Integration, Research Trends, India, 1992, p. 231, and references therein.
[6] F. Argoul, E. Freysz, A. Kuhn, C. Léger, L. Potin, Phys. Rev. E 53 (1996) 1777.
[7] J.R. de Bruyn, Phys. Rev. E 56 (1997) 3326.
[8] I. Rey, J.-L. Bruneel, J. Grondin, L. Servant, J.-C. Lassègues, J. Electrochem. Soc. 145 (1998) 3034.
[9] I. Rey, Thesis, Université Bordeaux I, France, 1997.
[10] C. Brissot, M. Rosso, J.-N. Chazalviel, P. Baudry, S. Lascaud, Electrochim. Acta 43 (1998) 1569.
[11] M. Doyle, T.F. Fuller, J. Newman, J. Electrochem. Soc. 140 (1993) 1526.
[12] C. Brissot, M. Rosso, J.-N. Chazalviel, S. Lascaud, J. Electrochem. Soc. 146 (1999) 4393.
[13] S. Lascaud, M. Perrier, A. Vallée, S. Besner, J. Prud'homme, M. Armand, Macromolecules 27 (1994) 7469.
[14] S. Lascaud, Ph.D. Thesis, Université de Montréal, Montréal, Que., Canada, 1996.
[15] C. Labrèche, I. Lévesque, J. Prud'homme, Macromolecules 29 (1996) 7795.
[16] C. Brissot, Thesis, Ecole Polytechnique, Palaiseau, France, 1998.
[17] M. Armand, W. Gorecki, R. Andréani, in: B. Scrosati, (Ed.), Proceedings of the Second International Symposium on Polymer Electrolytes, Elsevier, London, 1990, p. 91.
[18] L. Reibel, S. Bayoudh, P. Baudry, H. Majastre, Electrochim. Acta 43 (1998) 1171.
[19] S. Bayoudh, Thesis, Université Louis Pasteur, Strasbourg, France, 1997.
[20] P.G. Bruce, C.A. Vincent, J. Electroanal. Chem. 225 (1987) 1.
[21] A.J. Bard, L.R. Faulkner, Electrochemical Methods. Fundamentals and Applications, Wiley, New York, 1980.
[22] M. Rosso, J.-N. Chazalviel, V. Fleury, E. Chassaing, Electrochim. Acta 39 (1994) 507.
[23] H.J.S. Sand, Philos. Mag. 1 (1901) 45.
[24] I. Albinsson, B.-E. Mellander, J.R. Stevens, Solid State Ionics 60 (1993) 63.
[25] E. Peled, D. Golodnitsky, G. Ardel, V. Eshkenazy, Electrochim. Acta 40 (1995) 2197.
[26] D. Aurbach, E. Zinigrad, H. Teller, P. Dan, J. Electrochem. Soc. 147 (2000) 1274.
[27] V. Fleury, J.-N. Chazalviel, M. Rosso, Phys. Rev. Lett. 68 (1992) 2492.
[28] V. Fleury, J.-N. Chazalviel, M. Rosso, Phys. Rev. E 48 (1993) 1279.
[29] K.A. Linehan, J.R. de Bruyn, Can. J. Phys. 73 (1995) 177.
[30] C. Léger, J. Elezgaray, F. Argoul, Phys. Rev. Lett. 78 (1997) 5010.
[31] D.P. Barkey, D. Watt, Z. Liu, S. Raber, J. Electrochem. Soc. 141 (1994) 1206.
[32] C. Brissot, M. Rosso, J.-N. Chazalviel, S. Lascaud, J. Power Sources 81/82 (1999) 925.